Acta Pharmaceutica Sinica B 2025;15(3):1463–1479

Chinese Pharmaceutical Association
Institute of Materia Medica, Chinese Academy of Medical Sciences

Acta Pharmaceutica Sinica B

www.elsevier.com/locate/apsb
www.sciencedirect.com

ORIGINAL ARTICLE

Novel carbazole attenuates vascular remodeling through STAT3/CIAPIN1 signaling in vascular smooth muscle cells

Joo-Hui Han[a,*], Jong-Beom Heo[b], Hyung-Won Lee[c], Min-Ho Park[d], Jangmi Choi[d], Eun Joo Yun[b], Seongpyo Lee[c], Gyu Yong Song[b,*], Chang-Seon Myung[e,*]

[a]*College of Pharmacy and Research Institute of Pharmaceutical Sciences, Woosuk University, Wanju 55338, Republic of Korea*
[b]*College of Pharmacy, Chungnam National University, Daejeon 34134, Republic of Korea*
[c]*College of Pharmacy, Woosuk University, Wanju 55338, Republic of Korea*
[d]*Institute of Drug Research and Development, College of Pharmacy, Chungnam National University, Daejeon 34134, Republic of Korea*
[e]*Department of Pharmacology, College of Pharmacy, Chungnam National University, Daejeon 34134, Republic of Korea*

Received 19 July 2024; received in revised form 24 September 2024; accepted 22 October 2024

KEY WORDS

Atherosclerosis;
Vascular smooth muscle cell;
Signal transducer and activator of transcription 3;
Cytokine induced apoptosis inhibitor 1;
Janus tyrosine kinase 2;
Phenotyping switching;
Krüppel-like factor 4;
Carbazole

Abstract This study investigated the molecular mechanism of phenotypic switching of vascular smooth muscle cells (VSMCs), which play a crucial role in vascular remodeling using 9*H*-Carbazol-3-yl 4-aminobenzoate (CAB). CAB significantly attenuated platelet-derived growth factor (PDGF)-induced VSMC proliferation and migration. CAB suppressed PDGF-induced STAT3 activation by directly binding to the SH2 domain of STAT3. Downregulation of STAT3 phosphorylation by CAB attenuated CIAPIN1/JAK2/STAT3 axis through a decrease in CIAPIN1 transcription. Furthermore, abrogated CIAPIN1 decreased KLF4-mediated VSMC dedifferentiation and increased CDKN1B-induced cell cycle arrest and MMP9 suppression. CAB inhibited intimal hyperplasia in injury-induced neointima animal models by inhibition of the CIAPIN1/JAK2/STAT3 axis. However, CIAPIN1 overexpression attenuated CAB-mediated suppression of VSMC proliferation, migration, phenotypic switching, and intimal hyperplasia. Our study clarified the molecular mechanism underlying STAT3 inhibition of VSMC phenotypic

*Corresponding authors.
E-mail addresses: hanjh5621@woosuk.ac.kr (Joo-Hui Han), gysong@cnu.ac.kr (Gyu Yong Song), cm8r@cnu.ac.kr (Chang-Seon Myung).
Peer review under the responsibility of Chinese Pharmaceutical Association and Institute of Materia Medica, Chinese Academy of Medical Sciences.

https://doi.org/10.1016/j.apsb.2024.12.035

switching and vascular remodeling and identified novel active CAB. These findings demonstrated that STAT3 can be a major regulator to control CIAPIN1/JAK2/STAT3 axis that may be a therapeutic target for treating vascular proliferative diseases.

1. Introduction

Abnormal proliferation and migration of vascular smooth muscle cells (VSMCs) leads to neointima formation and vascular remodeling, followed by atherosclerotic progression[1,2]. Most VSMCs in the arterial tunica media display a contractile phenotype, which allows them to maintain vascular tone, blood pressure, and blood flow distribution to tissues[3]. However, VSMCs can phenotypically switch and are considered to be a key mechanism in arterial remodeling[4]. VSMCs transit from a contractile phenotype to a synthetic phenotype (VSMC dedifferentiation) in response to vascular injury and stimulation of growth factors such as platelet-derived growth factors (PDGFs)[5-7]. Synthetic-state VSMCs actively proliferate and migrate into the arterial intima, leading to vascular proliferative diseases such as atherosclerosis, postangioplasty restenosis, and failure of arterial bypass grafts[8,9]. Thus, it is essential to investigate the molecular mechanisms underlying VSMC phenotypic switching to identify novel therapeutics for atherosclerosis and related cardiovascular disorders.

Signal transducer and activator of transcription 3 (STAT3) signaling pathway affects various biological processes, such as cell differentiation, proliferation, and apoptosis[10]. STAT3 activation is vital as a transcription factor to regulate downstream gene expression[11-15]. Although STAT3 is critically involved in vascular injury, the underlying mechanisms of how STAT3 regulates VSMC phenotypic switching remain poorly understood, and the functional importance of suppressing these pathways by novel inhibitors during the development of vascular proliferative diseases has not been demonstrated.

We previously reported that cytokine-induced apoptosis inhibitor 1 (CIAPIN1) induced VSMC dedifferentiation and promoted neointima formation increasing of Janus kinase 2 (JAK2) and STAT3 activation[16]. PDGF receptor-beta (PDGFR-β) pathways affect CIAPIN1 expression, but the underlying mechanisms and upstream molecules that regulate CIAPIN1 remain unclear.

Carbazole and its derivatives are an important nitrogen-containing aromatic heterocyclic compound easily introduced into the structurally rigid carbazolyl ring[17]. In addition, carbazole is an “advantageous scaffold” containing desirable electronic and charge-transport properties since it reacts with many receptors and can bind reversibly to proteins and enzymes, providing an opportunity to study and develop novel drugs that target one or more biological structures[18,19]. Through these characteristics, carbazole derivatives have been reported to have various biological activities, such as anticancer[20], antimicrobial[21], antioxidants[22], and anti-inflammatory[23] activities. In our ongoing search for novel synthesized compounds that attenuate vascular remodeling by inhibiting STAT3, we found that the 9*H*-Carbazole derivatives inhibited STAT3 activation.

In this study, we investigated the therapeutic effects of 9*H*-Carbazol-3-yl 4-aminobenzoate (CAB) on vascular remodeling by regulating VSMC phenotypic switching, proliferation, migration, and the pathogenesis of neointima formation. Our findings showed the inhibitory effects of CAB on STAT3 activation through direct binding in the Src homology 2 (SH2) domain. In addition, a decrease in STAT3 activity inhibits CIAPIN1 transcription by affecting its promoter activation. These effects suppress CIAPIN1/JAK2/STAT3 axis to inhibit Krüppel-like factor 4 (KLF4)-mediated VSMC dedifferentiation. Moreover, CAB-mediated STAT3 inhibition promoted cyclin-dependent kinase inhibitor 1B (CDKN1B) transcription as a functional cell cycle regulator[24], resulting in decreased VSMC proliferation and migration. Therefore, the physiological impacts of the identified targets were corroborated in arterial tissues from neointima lesions.

2. Materials and methods

2.1. Animals and drug administration

Sprague−Dawley rats (SD rats, male, 10-weeks-old, 380−420 g) and C57BL/6 mice (male, 6-weeks-old, average 23 g) were obtained from Samtako (Osan, Korea). The animals were housed two per cage. They fed a standard maintenance diet (1314 FORTIFIED, Altromin, Lage, Germany) *ad libitum* in the animal facility under controlled temperature (22 ± 2 °C), humidity (50 ± 5%), and lighting (12/12 h dark−light cycle, lights on at 7:00 a.m.) conditions. Animal experiments were approved by the Institutional Animal Care and Use Committee of Chungnam National University (202012A-CNU-192) and Woosuk University (WS-2023-10). Animals’ protocols were performed in accordance with the Guide for the Care and Use of Laboratory Animals published by the US National Institutes of Health. After a 1-week acclimatization period, rats were randomly divided into five groups (n = 7 in each group): sham, balloon injury (BI) and BI with 20 mg/kg CAB, rat CIAPIN1 transduction (rCIA1), rCIA1, BI with 20 mg/kg CAB. After 1 day of balloon injury to induce neointima formation, rats were orally administered CAB dissolved in 0.5% carboxymethyl cellulose (CMC, C5678, Sigma−Aldrich) daily. The body weight of the rats was recorded on the indicated days for CAB toxicity (Supporting Information Fig. S7A). Mice were randomly divided into three groups (n = 6 in each group): sham, carotid ligation (LI), and LI with 3 mg/kg CAB. The mouse dosage was converted from the rat dosage using Meeh’s constant for total body surface area (TBSA) as Eq. (1)[25]:

$$\mathrm{TBSA} = K \times \mathrm{weight}^{2/3} \tag{1}$$

The average weight of the rats used in our study was approximately 400 g, with a K value set at 9.83 based on a previous study[26]. Similarly, the average weight of the mice was 23 g, with a K value of 9.82, referenced from another study[27]. We calculated the appropriate dosage for mice as 2.98 mg/kg, rounded to 3 mg/kg for administration, as shown in Eq. (2):

$$\text{Mouse equibalent dose} = \frac{9.82 \times (23\ \text{g})^{2/3}}{9.83 \times (400\ \text{g})^{2/3}} \times 20\ \text{mg/kg} \tag{2}$$

After 1 day of carotid ligation to induce neointima formation, mice were orally administered with CAB dissolved in 0.5% CMC daily.

2.2. *Induction of neointima formation and morphometric analysis*

To induce neointima formation, we carried out balloon injury in rat carotids[28-30] and carotid ligation in a mouse model[31], as described previously. The balloon injury in the rat carotid artery was performed using SD rats. Briefly, rats were anesthetized *via* an intraperitoneal injection of pentobarbital sodium (50 mg/kg body weight). A balloon catheter (Fogarty 2F, Edwards Lifesciences, CA, USA) was inserted into the left common carotid artery *via* the external carotid artery. Then, the inflated balloon was drawn gently toward the external carotid artery. After this procedure was repeated five times, the catheter was removed, and the injured artery was washed with saline. Then, 50 μL of lentiviral vectors (2×10^9 plaque-forming units/mL) expressing control vector (Con) or rat *Ciapin1* (rCIAPIN1 or rCIA1) were incubated into the injured artery for 30 min. The ligation of the mouse carotid artery was performed using the C57BL/6 mouse. Mice were anesthetized *via* an intraperitoneal injection of pentobarbital sodium (50 mg/kg body weight). After we closed the wound using skin sutures and swabbed all sides of the closed wound with povidone-iodine, the rats and mice were allowed to recover while being kept warm and pain-free on a heated pad by treatment with 1% ketoprofen (0.2 mL/kg) subcutaneously. After 14 or 28 days, all animals were anesthetized by CO_2 administration, following a gradual CO_2 displacement protocol as outlined in the American Veterinary Medical Association Guidelines for the Euthanasia of Animals: 2020 Edition (typically at 30%−70% chamber volume per minute) while monitoring the animals for signs of distress, and their arteries, liver, heart, lung, and kidney tissues were collected and stored at −80 °C until further analysis for qPCR and Western blotting or embedded in paraffin for histological analysis.

The tissues were fixed with 4% paraformaldehyde and embedded in paraffin. Then, the tissues were cut into 4-μm-thick sections. The sections were stained with hematoxylin and eosin (H&E), images were acquired using a microscope (Nikon Eclipse Ti, Nikon Instruments, Inc., Tokyo, Japan), and histological analysis was performed using AxioVision (Version 4.8.3, Carl Zeiss Microscopy, White Plains, NY, USA). The area of the residual lumen and the areas circumscribed by the internal and external elastic lamina were measured to determine the intima and media areas. The degree of neointimal thickening was assessed using the intima-to-media area ratio and the intimal area. *In vivo* studies were performed in a blinded fashion at the drug administration and histological stages. For the quantification of tissue staining and pathological evaluation of animal specimens, the investigator was blinded to ensure an unbiased interpretation of the results.

2.3. *Immunohistochemistry*

Immunohistochemical assays for proliferating cell nuclear antigen (PCNA) were performed in rat carotid artery sections. The sections were subjected to antigen retrieval using a 10 mmol/L sodium citrate buffer (pH 6.0) and incubated for 10 min in a 3% hydrogen peroxide (H_2O_2) solution to quench endogenous peroxidase activity. After the sections were incubated in blocking buffer (5% goat serum in phosphate buffered saline) for 1 h at room temperature, they were treated with PCNA antibody diluted in antibody diluent (Dako, Glostrup, Denmark) overnight at 4 °C, followed by incubation with biotin-conjugated secondary antibodies. Staining signals were detected using a standard avidin-biotin complex-peroxidase system (Vector Laboratories, CA, USA). Subsequently, positive antibody binding was visualized using a 3,3′-diaminobenzidine substrate (Vector Laboratories, CA, USA), followed by hematoxylin counterstaining. Immunohistochemistry staining levels were quantified using ImageJ software (Version 1.53c).

2.4. *Statistical analyses*

All data are expressed as the mean ± standard deviation (SD) of at least 3−5 independent experiments. Statistical analyses were performed with GraphPad Prism software (Version 10, San Diego, CA, USA). The normality of the data distributions was tested using the Shapiro−Wilk test. A two-sided, unpaired Student's t-test was used to analyze the difference between two data groups with normally distributed variables. Differences among three or more groups were analyzed with one-way analysis of variance (ANOVA) followed by a *post hoc* Bonferroni's test if F achieved statistical significance ($P < 0.05$) and there was no significant variance in homogeneity with Bartlett's test. Differences with $P < 0.05$ were considered statistically significant.

3. Results

3.1. *Identification of active 9H-Carbazole derivatives to inhibit PDGF-BB-induced vascular remodeling*

To validate drug-likeness and therapeutic efficacy, we designed and synthesized a library of four 9*H*-Carbazole derivatives by modifying the C-4 position moiety of benzoate, which was linked to the C-3 position of the 9*H*-Carbazole moiety (Supporting Information Fig. S1A). To assess the effects of the 9*H*-Carbazole derivatives on PDGF-BB-induced VSMC proliferation, we treated cells with 5 μmol/L derivatives for 2 h, followed by PDGF-BB (25 ng/mL) for 24 h. As shown in Fig. S1B, the derivatives, including CAB, 2, 3, and 4, significantly inhibited PDGF-BB-stimulated VSMC proliferation. Among them, CAB exhibited the most potent inhibitory activity on PDGF-BB-induced VSMC proliferation, suggesting that a free amino group at the C-4 position of benzoate plays an important role in the inhibitory activity.

Since CAB exhibited the most significant inhibitory activity on PDGF-BB-induced VSMC proliferation at the lowest IC_{50} compared to other CAB derivatives (Supporting Information Table S1), we performed further studies using CAB (Fig. 1A). CAB (1−5 μmol/L) dose-dependently inhibited PDGF-BB-induced VSMC proliferation (Fig. 1B). Exposure to the highest concentration of CAB (5 μmol/L) did not induce cytotoxic effects in VSMCs compared to H_2O_2 (1 mmol/L), which is a major reactive oxygen species causing cell death *via* apoptosis (Fig. 1C and D)[32]. In

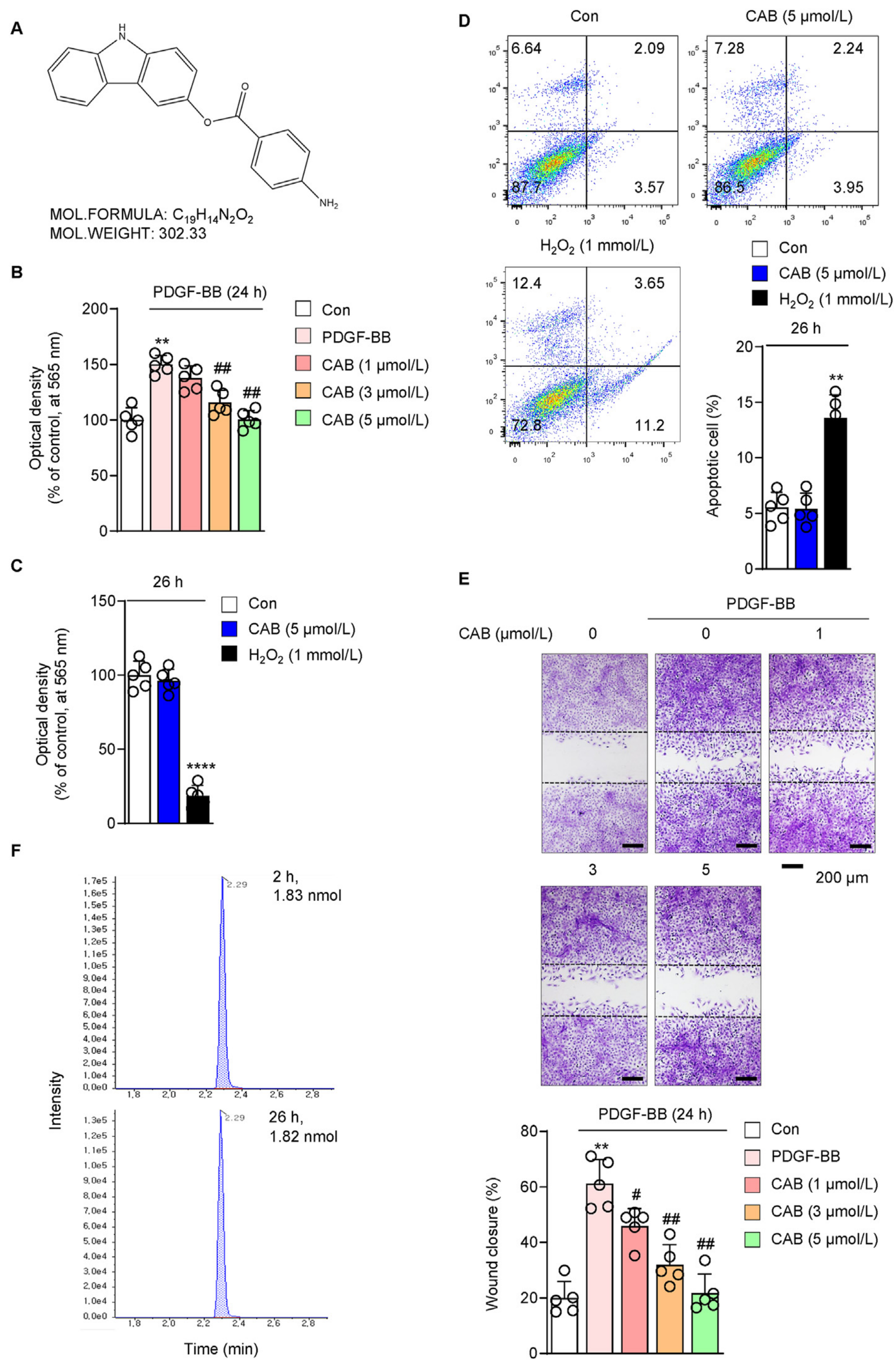

Figure 1 Inhibitory effect of CAB on PDGF-BB-induced VSMC proliferation and migration. (A) Chemical structure of 9*H*-Carbazol-3-yl 4-aminobenzoate (CAB). (B) MTT assay showing the effect of CAB (1−5 μmol/L) on PDGF-BB-induced VSMC proliferation ($n = 5$ per group). (C) MTT assay showing the cytotoxicity of CAB (5 μmol/L) and H_2O_2 (1 mmol/L, positive control) in VSMCs after 26 h ($n = 5$ per group). (D) Effect of CAB (5 μmol/L) on VSMCs apoptosis. Cells were treated with CAB (5 μmol/L) for 26 h ($n = 5$ per group). (E) Wound healing assay showing the effect of CAB (1−5 μmol/L) on PDGF-BB-induced VSMC migration ($n = 5$ per group). (F) Representative extracted ion chromatogram for quantification of the intracellular CAB concentration from VSMCs after 2 or 26 h. *P*-values were determined by the ANOVA followed by a *post hoc* Bonferroni's test. $^{**}P < 0.01$ and $^{****}P < 0.0001$ *vs*. Con, $^{\#}P < 0.05$ and $^{\#\#}P < 0.01$ *vs*. PDGF-BB. The data are the mean ± SD.

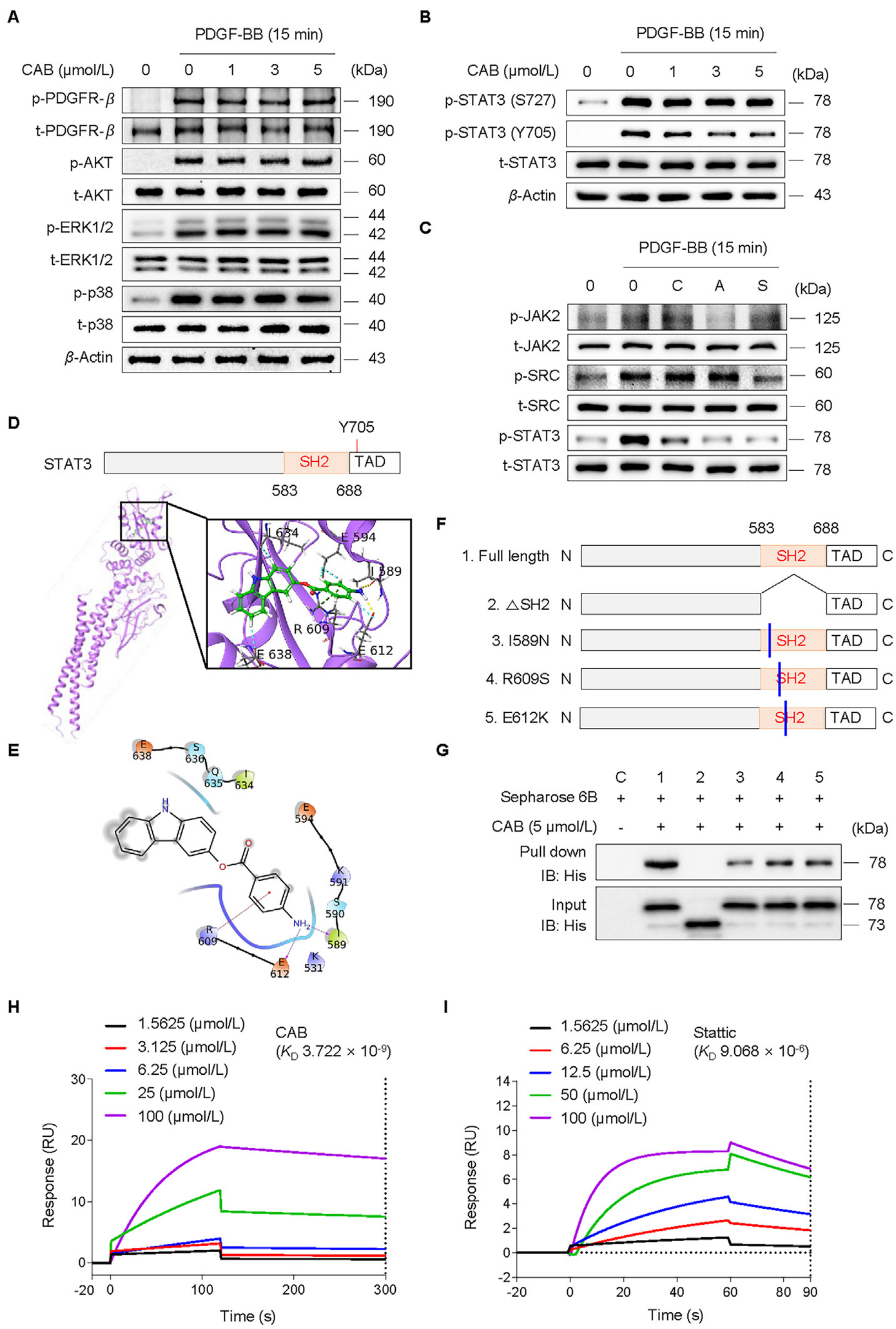

Figure 2 Inhibitory effect of CAB on PDGF-BB-induced STAT3 activation in VSMCs. (A) Effect of CAB (1−5 μmol/L) on PDGFR-*β*, AKT, ERK1/2, and p38 phosphorylation in the PDGF-BB-induced VSMCs for 15 min. (B) Effect of CAB (1−5 μmol/L) on STAT3 phosphorylation in the PDGF-BB-induced VSMCs for 15 min Ser727: S727, Tyr705: Y705. (C) Effect of CAB (5 μmol/L), AG490 (20 μmol/L), and SU6656 (2 μmol/L) on JAK2, SRC, and STAT3 phosphorylation in the PDGF-BB-induced VSMCs for 15 min. (D) Docking results of the STAT3 SH2 domain (PDB accession number: 6TLC) in complex with CAB. STAT3 and CAB are shown in purple ribbon and green stick models, respectively. The surrounding residues associated with the CAB are shown in the gray stick model. The overall SH2 domain structure and magnified view of the binding pocket are shown. TAD: transactivation domain. (E) Ligand interaction diagrams of CAB docked to the STAT3 SH2 domain (PDB accession number: 6TLC). The 2D structure of CAB is drawn in a black line. The residues interacting with the compound are surrounded with pink arrows indicating three hydrogen bonds (I589, R609, and E612). (F) Schematic domain structures of STAT3 recombinant proteins. ΔSH2: SH2 deletion, I589N: Ile589 to Asn589, R609S: Arg609 to Ser609, E612K: Glu612 to Lys612. (G) His-tag pull-down assay with deletion and point mutation of predicted binding sites of STAT3 whether CAB binds to SH2 of STAT3. C: the group of full-length STAT3 protein mixed with CAB unconjugated Sepharose 6B. (H, I) Surface plasmon resonance (SPR) analysis of CAB or stattic binding to the STAT3 protein. The graph illustrates the sensorgram results for different concentrations of CAB (1.5625, 3.125, 6.25, 25, and 100 μmol/L) and stattic (1.5625, 6.25, 12.5, 50, and 100 μmol/L) binding to immobilized STAT3 protein (amino acids 127−688). The response (RU) is plotted against time (seconds), showing

Table 1 Kinetic parameters resulting from surface plasmon resonance (SPR) analysis with CAB and stattic bind to the STAT3 protein.

Compd.	Surface plasmon resonance (SPR)		
	K_a [/mol/L/s]	K_d [/s]	K_D [mol/L]
CAB	1.602×10^5	5.964×10^{-4}	3.722×10^{-9}
Stattic	1.002×10^3	9.083×10^{-3}	9.068×10^{-6}

K_a: association rate constant, K_d: dissociation rate constant, K_D: equilibrium constant.

addition, there were no signs of cell apoptosis induction by CAB compared with the control, indicating that CAB-mediated inhibition of VSMC proliferation was not due to toxic effects. In addition, CAB treatment significantly inhibited PDGF-BB-induced proliferation of human aortic smooth muscle cells, as observed in VSMCs, without inducing cytotoxicity (Fig. S1C and S1D).

VSMC migration as well as proliferation are critical processes for vascular remodeling in response to arterial injury or mitogenic factors[33]. To examine the effects of CAB on VSMC migration, we performed a wound healing assay in CAB-treated VSMCs. VSMC migration occurred upon PDGF-BB stimulation, while CAB treatment significantly lowered VSMC migration compared to the control (Fig. 1E).

Given that CAB attenuates VSMC proliferation and migration, we examined whether CAB can be intracellularly enriched in VSMCs to affect cellular function. In the VSMCs treated with the highest concentration of CAB (5 μmol/L), CAB was extracted by acetonitrile, and liquid chromatography−quadrupole time-of-flight tandem mass spectrometry measured the cellular CAB concentration. The intracellular CAB amounts estimated from a standard curve were 1.83 ± 0.66 and 1.82 ± 0.62 nmol/10^5 cells after treatment for 2 and 26 h, respectively, indicating that CAB was promptly taken up by the cells, and the concentration was maintained until 26 h (Fig. 1F). Given the average volume of a single cell (≈5 pL)[34], the actual CAB concentration per cell reached ≈3.67 mmol/L, implying that intracellular pharmacokinetics (PK) of CAB may affect the disease phenotype. Taken together, these results identify a role of CAB in VSMC proliferation and migration without cytotoxicity.

3.2. *CAB specifically inhibits STAT3 phosphorylation by binding to SH2 domain in PDGF-BB-induced VSMCs*

In the early stages of intima hyperplasia, PDGF-BB binds to its receptor, PDGFR-β, to trigger phosphorylation of downstream pathways, including protein kinase B (AKT/PKB), extracellular signal-regulated kinase 1/2 (ERK1/2), p38, JAK2, and STAT3[35-38]. To explore the underlying molecular mechanism of CAB activity, we determined whether CAB functioned by affecting PDGFR-β pathways. The results of Fig. 2A show that CAB did not affect PDGF-BB-stimulated PDGFR-β, AKT, ERK1/2, and p38 phosphorylation. However, CAB significantly inhibited PDGF-BB-induced STAT3 tyrosine (Tyr) 705 phosphorylation without affecting the serine (Ser) 727 residue, which is a downstream active MAPK signaling residue (Fig. 2B and Supporting Information Fig. S2A)[39,40]. Since angiotensin II (Ang II) or IL-6 induce VSMC proliferation by activating STAT3[41,42], we found CAB (3−5 μmol/L) inhibited Ang II or IL-6 induced VSMC proliferation (Fig. S2B).

Since STAT3 Tyr705 residue is regulated by JAK2 or Src proto-oncogene (SRC)[43,44], we examined the effect of CAB on JAK2 and SRC phosphorylation in PDGF-BB-induced VSMCs using AG490 (JAK2 inhibitor) or SU6656 (SRC inhibitor). As shown in Fig. 2C and Fig. S2C, CAB did not inhibit PDGF-BB-induced JAK2 and SRC phosphorylation unlike AG490 and SU6656, implying a direct function to STAT3.

Given that CAB inhibits STAT3 phosphorylation without affecting upstream molecules, we hypothesized that CAB regulated STAT3 by direct inhibition. We performed a ligand-docking assay using crystal structure to detect the docking possibility of CAB in the STAT3. Through the docking study, CAB showed interactions with STAT3 at residues Ile589, Arg609, and Glu612 in the SH2 domain, which is necessary for receptor association and tyrosine phosphodimer formation (STAT3 docking score: −3.25 kcal/mol) (Fig. 2D and E)[45]. His-tag pull-down assays were performed to further elucidate the interaction between CAB and the SH2 of STAT3. Briefly, a series of His-STAT3-fusion protein-expressing vectors with different domains, as well as Ile589, Arg609, and Glu612 mutant (Fig. 2F), were constructed and used to investigate whether SH2 is the specific binding site for CAB. The result showed that CAB-conjugated beads did not pull down STAT3 fragments lacking SH2, whereas full-length was successfully pulled down by CAB-conjugated beads (Fig. 2G). In addition, surface plasmon resonance (SPR) analysis demonstrated that CAB binds to the STAT3 protein (amino acids 127−688) in a concentration-dependent manner (Fig. 2H). The sensorgram displayed distinct association and dissociation phases for each concentration of CAB (1.5625, 3.125, 6.25, 25, and 100 μmol/L) or stattic (Fig. 2I) tested (1.5625, 6.25, 12.5, 50, and 100 μmol/L). As the concentration of CAB or stattic increased, the response units (RU) also increased, indicating a higher binding affinity at higher concentrations. The binding interaction of CAB was quantified with an association rate constant (K_a) of 1.602×10^5/mol/L/s, a dissociation rate constant (K_d) of 5.964×10^{-4}/s, and an equilibrium constant (K_D) of 3.722×10^{-9} mol/L. In contrast, the binding interaction of stattic was quantified with an association rate constant of 1.002×10^3/mol/L/s, a dissociation rate constant of 9.083×10^{-3}/s, and an equilibrium constant of 9.068×10^{-6} mol/L (Table 1). Thus, the interaction between CAB and the STAT3 protein was more substantial than that of stattic, which is previously known as a STAT3 inhibitor[46], indicating the potential of CAB as a more potent STAT3 inhibitor.

These findings suggested that CAB could directly bind to STAT3, and its binding site was likely located in the SH2 of STAT3. Furthermore, CAB did not bind to STAT3 strongly compared to full-length when Ile59, Arg609, and Glu612 in the SH2 were mutated, suggesting that those residues in SH2 are critical for direct binding between CAB and STAT3.

3.3. *CAB inhibits STAT3 activation as a transcription factor in PDGF-BB-induced VSMCs*

In accordance with the docking results, CAB (3−5 μmol/L) inhibited STAT3 dimerization, and this inhibitory effect was

the association and dissociation phases for each concentration. The binding interaction was characterized by an equilibrium constant (K_D) of CAB and stattic (3.722×10^{-9} mol/L and 9.068×10^{-6} mol/L, respectively), indicating the affinity between CAB and the STAT3 protein.

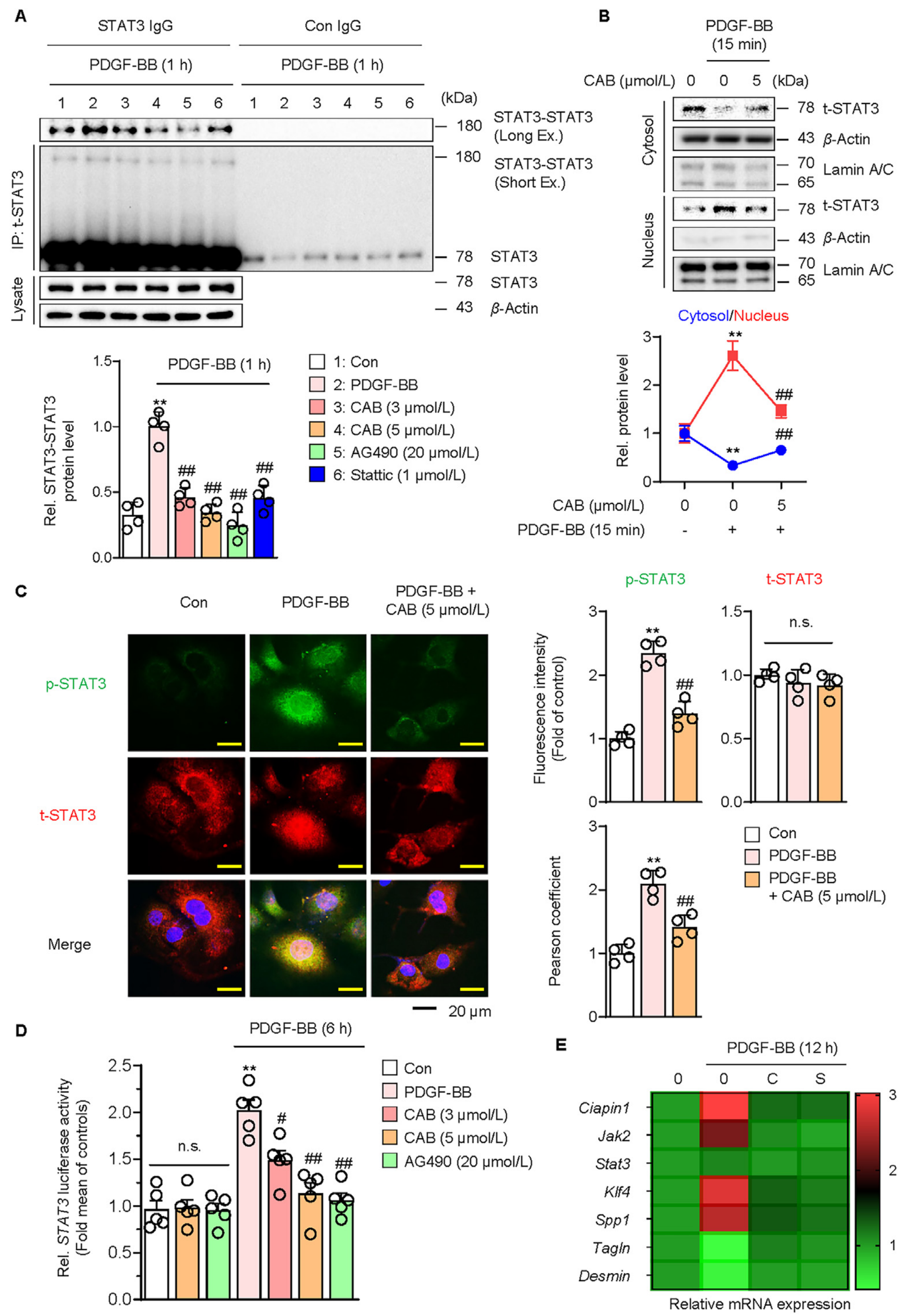

Figure 3 Inhibitory effect of CAB on PDGF-BB-induced STAT3 transcriptional activity in VSMCs. (A) Effect of CAB (3−5 μmol/L), AG490 (20 μmol/L) and stattic (1 μmol/L) on STAT3 dimerization in the PDGF-BB-induced VSMCs. Immunoblot of STAT3 monomers and dimers using STAT3 or control (Con) IgG (n = 4 per group). 1: Con, 2: PDGF-BB, 3: CAB (3 μmol/L), 4: CAB (5 μmol/L), 5: AG490 (20 μmol/L), and 6: Stattic (1 μmol/L) Short Ex.: short exposure, Long Ex.: long exposure (B) Effect of CAB on STAT3 nuclear translocation in the PDGF-BB-induced VSMCs for 15 min. The cells were fractionated into cytosolic and nuclear compartments as described in the Methods section (n = 4 per group). (C) Fluorescence images (left) and quantification data (right) of p-STAT3 and t-STAT3 in the PDGF-BB-induced VSMCs for 15 min. The fluorescence intensities of FITC (*i.e.*, p-STAT3) and TRITC (*i.e.*, t-STAT3) were quantified using ImageJ software. Colocalization of TRITC and DAPI (*i.e.*, nuclei) was analyzed using the Pearson correlation coefficient (n = 4 per group). Scale bars: 20 μm. (D) Luciferase activities of STAT3 in the CAB-treated VSMCs after PDGF-BB stimulation for 6 h (n = 5 per group). The level of STAT3 binding promoter-reporter firefly luciferase activity is indicated relative to the activity of the *Renilla* luciferase control. (E) Heatmap of the mRNA expression of the indicated genes with or without CAB (5 μmol/L) or stattic (1 μmol/L) in the PDGF-BB-induced VSMCs for 24 h (n = 4 independent experiments). P-values were determined by the ANOVA followed by a *post hoc* Bonferroni's test. $^{**}P < 0.01$ *vs*. Con, $^{\#}P < 0.05$ and $^{\#\#}P < 0.01$ *vs*. PDGF-BB. n.s.: not significant. The data are the mean ± SD.

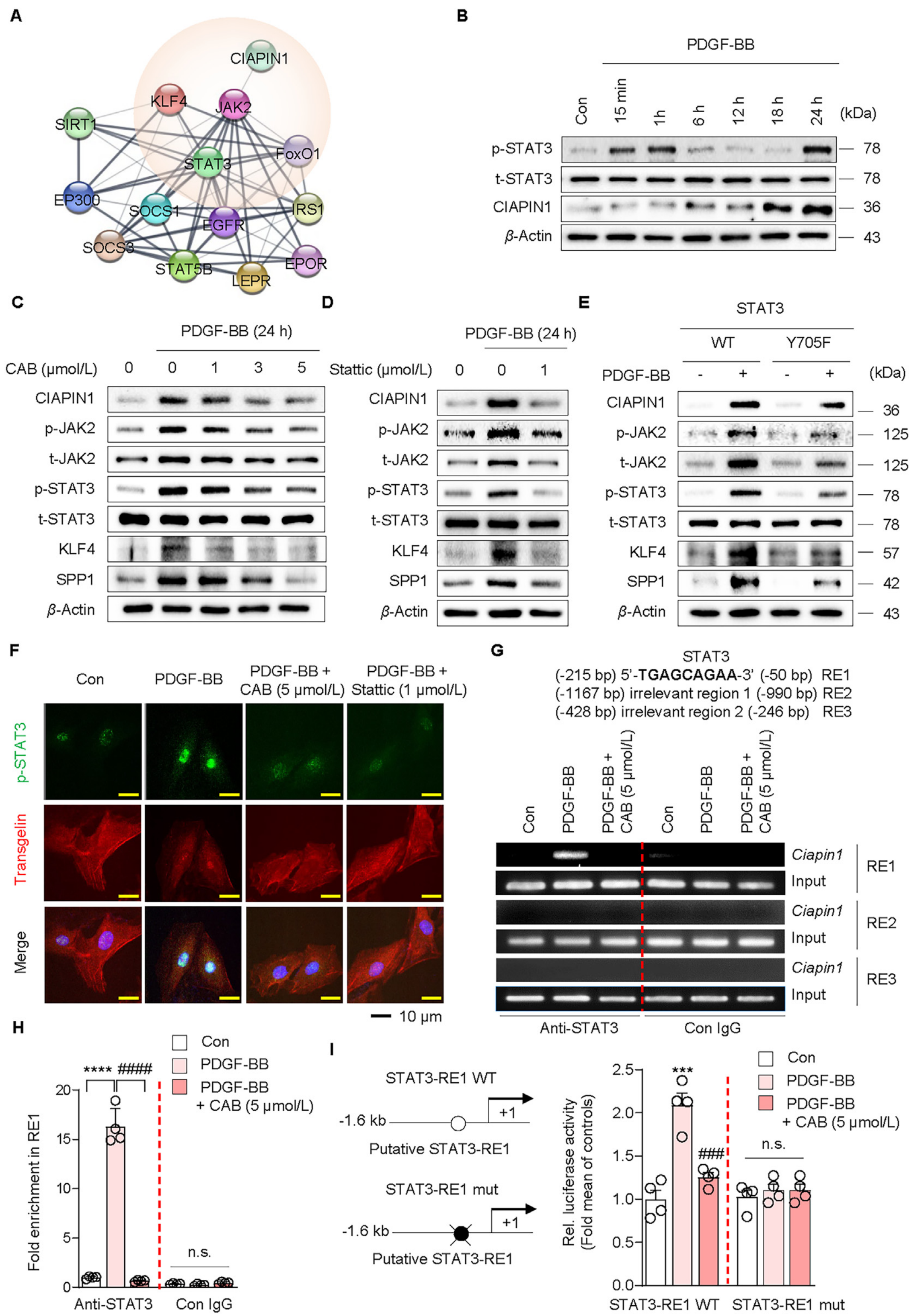

Figure 4 Inhibitory effect of CAB on PDGF-BB-induced CIAPIN1/JAK2/STAT3/KLF4 regulatory networks in VSMCs. (A) STAT3-associated protein networks generated using the STRING database. (B) Effect of PDGF-BB on STAT3 phosphorylation and CIAPIN1 expression until 24 h in VSMCs. Effect of (C) CAB (1−5 μmol/L), (D) stattic (1 μmol/L), (E) STAT3 Tyr705 mutant (Y705F) on CIAPIN1, *p*-JAK2, t-JAK2, p-STAT3, t-STAT3, KLF4 and SPP1 expression in the PDGF-BB-induced VSMCs for 24 h. WT: wild-type (F) Fluorescence images of p-STAT3 (Tyr705) and transgelin in the PDGF-BB-induced VSMCs for 24 h. The fluorescence intensities (Supporting Information Fig. S5) of FITC (*i.e.*, p-STAT3) and TRITC (*i.e.*, transgelin) were quantified using ImageJ software ($n = 4$ per group). Scale bars: 10 μm. (G) Representative images of the chromatin immunoprecipitation (ChIP)-PCR assay evaluated the binding of STAT3 to CIAPIN1 promoter in VSMCs treated with CAB for 2 h, followed by stimulation with PDGF-BB for 6 h. ChIP was performed with anti-STAT3 antibody and normal rabbit IgG. The PCR amplifications

similar to AG490 and stattic (STAT3 inhibitor) (Fig. 3A and Supporting Information Fig. S3). Since tyrosine-phosphorylated and dimerized STAT3 triggers nuclear translocation to function as a transcription factor[47], we examined the effect of CAB on PDGF-BB-induced STAT3 nuclear translocation using cellular fractions and immunofluorescence. PDGF-BB increased STAT3 phosphorylation and nuclear translocation; however, CAB blocked these phenomena (Fig. 3B and C). To assess transcriptional activity, we transfected VSMCs with the luciferase reporter, which consisted of four copies of the STAT3 binding site in a minimal promoter. We observed that CAB inhibited PDGF-BB-induced STAT3 DNA binding activity, similar to JAK2 inhibition (AG490) (Fig. 3D).

These results led us to hypothesize that CAB regulated the transcription of STAT3 downstream genes to regulate VSMC proliferation, migration, and phenotypic switching. Thus, we measured the mRNA levels of *Ciapin1*, *Jak2*, *Stat3*, *Klf4*, secreted phosphoprotein 1 (*Spp1*), Transgelin (*Tagln*), and *Desmin* and observed that CAB significantly restored the alteration of mRNA levels (Fig. 3E). These findings, together with those shown above, reinforce the idea that CAB suppresses PDGF-BB-induced activation of STAT3 as a transcription factor.

3.4. CAB inhibits PDGF-BB-induced CIAPIN1/JAK2/STAT3 activation to regulate VSMC phenotypic switching

Next, we examined a series of proteins involved in the STAT3 pathways using the STRING database. In the protein network analysis, CIAPIN1 and KLF4 were found to be interconnected with a subset of proteins (Fig. 4A). Of those linked to the core network, the proteins were associated with VSMC phenotypic switching[16,48]. Interestingly, we found STAT3 phosphorylation was increased at the early time (15 min−1 h) and subsequently late time (24 h) point, indicating early time activated STAT3 functions to increase in CIAPIN1 expression as a transcription factor (Fig. 4B and Supporting Information Fig. S4), and CIAPIN1 may affect STAT3 phosphorylation through JAK2 upregulation[16].

To verify the effect of CAB on associated protein regulation, we first examined the levels of CIAPIN1, JAK2, and STAT3 activation in PDGF-BB-induced VSMCs to examine the alteration of CIAPIN1/JAK2/STAT3 axis. As shown in Fig. 4C and Supporting Information Fig. S5A, CAB significantly inhibited PDGF-BB-stimulated CIAPIN1 and JAK2 expression. Owing to the alteration of the total JAK2 level, phosphorylation of JAK2 and STAT3, the JAK2 downstream molecule, was attenuated by CAB treatment. To determine whether STAT3 regulates CIAPIN1/JAK2/STAT3 signaling pathway *via* an autoregulatory circuit, we introduced stattic and STAT3 Tyr705 mutant (Y705F). As shown in Fig. 4D and Fig. S5B, stattic significantly inhibited PDGF-BB-induced CIAPIN1 and JAK2 expression, and JAK2 and STAT3 phosphorylation. Furthermore, STAT3 Y705F abrogated PDGF-BB-induced CIAPIN1 and JAK2 expression, and JAK2 and STAT3 phosphorylation, indicating that STAT3 plays a pivotal role in the CIAPIN1/JAK2/STAT3 autoregulatory circuit (Fig. 4E and Fig. S5C).

In response to vascular injury and other stimuli, such as growth factors, including PDGF, VSMCs actively proliferate and migrate into the arterial intima by VSMC dedifferentiation, switching from a contractile to a synthetic phenotype that results in neointima formation[4]. Since CIAPIN1 and STAT3 regulate VSMC dedifferentiation[16,49], we examined the effect of CAB on PDGF-BB-induced VSMC phenotypic switching. KLF4 is one of the corepressors that competes with myocardin activity to increase contractile genes for enhancing VSMC differentiation[50]. As shown in Fig. 4C and Fig. S5A, CAB decreased PDGF-BB-induced expression of KLF4 and SPP1, one of the synthetic phenotype markers. Similar to CAB, stattic and STAT3 Y705F inhibited KLF4 and SPP1 expression, indicating that STAT3 affects KLF4 to regulate VSMC phenotypic switching (Fig. 4D and E, Fig. S5B and S5C). In addition, PDGF-BB increased STAT3 phosphorylation mainly in the nucleus, but decreased the expression of transgelin, one of the contractile phenotype markers[51,52], indicating phenotypic transition from a contractile to a synthetic state (Fig. 4F and Fig. S5D). However, CAB treatment restored PDGF-BB-mediated alterations in STAT3 phosphorylation and transgelin by blocking VSMC dedifferentiation.

To elucidate the underlying mechanism of CIAPIN1 inhibition by CAB-mediated STAT3 suppression, we hypothesized that STAT3, as a transcriptional factor, contributes to the *CIAPIN1* gene transactivation. We postulated that a putative DNA-binding site would be present in the gene promoter. To elucidate this interaction *in situ*, we found a putative STAT3-binding site in the *Ciapin1* gene promoter (STAT3-RE1) using JASPAR 2024 (https://jaspar.elixir.no/). Then, we sought to evaluate the interaction with STAT3 and *Ciapin1* promoter by the chromatin immunoprecipitation (ChIP)-PCR assay. Using anti-STAT3 antibody, we immunoprecipitated protein/DNA complexes from VSMCs treated with CAB for 2 h, followed by stimulation with PDGF-BB for 6 h and amplified the putative interacting region of the endogenous rat *Ciapin1* promoter *via* PCR. While the binding of STAT3 to the *Ciapin1* promoter region significantly increased after stimulation with PDGF-BB, CAB treatment inhibited protein/DNA binding (Fig. 4G). The specificity of STAT3 binding was confirmed using franking primers targeting irrelevant regions in the promoter (STAT3-RE2 and -RE3). qPCR analysis verified STAT3 and STAT3-RE1 binding (Fig. 4H). Treatment of VSMCs with PDGF-BB significantly promoted luciferase expression from a reporter construct containing −1.6 kb *Ciapin1* gene, but CAB inhibited PDGF-BB-induced CIAPIN1 luciferase expression (Fig. 4I). However, the mutation of STAT3-RE1 abolished the upregulation of PDGF-BB-induced CIAPIN1 luciferase expression.

Taken together, these results demonstrate that STAT3, activated by PDGF-BB, transactivates the *Ciapin1* gene, which promotes VSMC dedifferentiation from contractile to synthetic phenotype. However, CAB blocks this phenotype.

were performed using the franking primers for the STAT3-response elements (REs). The specificity of STAT3 binding was verified using primers targeting irrelevant regions in the promoter. The input represents the electrophoresis of chromatin fragments that did not undergo immunoprecipitation. (H) qPCR assays for STAT3 and STAT3−RE1 binding. (I) Effect of STAT3−RE1 mutation on *Ciapin1* promoter reporter activity in PDGF-BB-induced VSMCs for 6 h ($n = 4$ per group). The data are presented as fold induction compared with the activity in control cells. P-values were determined by the ANOVA followed by a *post hoc* Bonferroni's test. $^{**}P < 0.01$, $^{***}P < 0.001$ and $^{****}P < 0.0001$ *vs*. Con, $^{\#\#}P < 0.01$, $^{\#\#\#}P < 0.001$ and $^{\#\#\#\#}P < 0.0001$ *vs*. PDGF-BB. n.s.: not significant. The data are the mean ± SD.

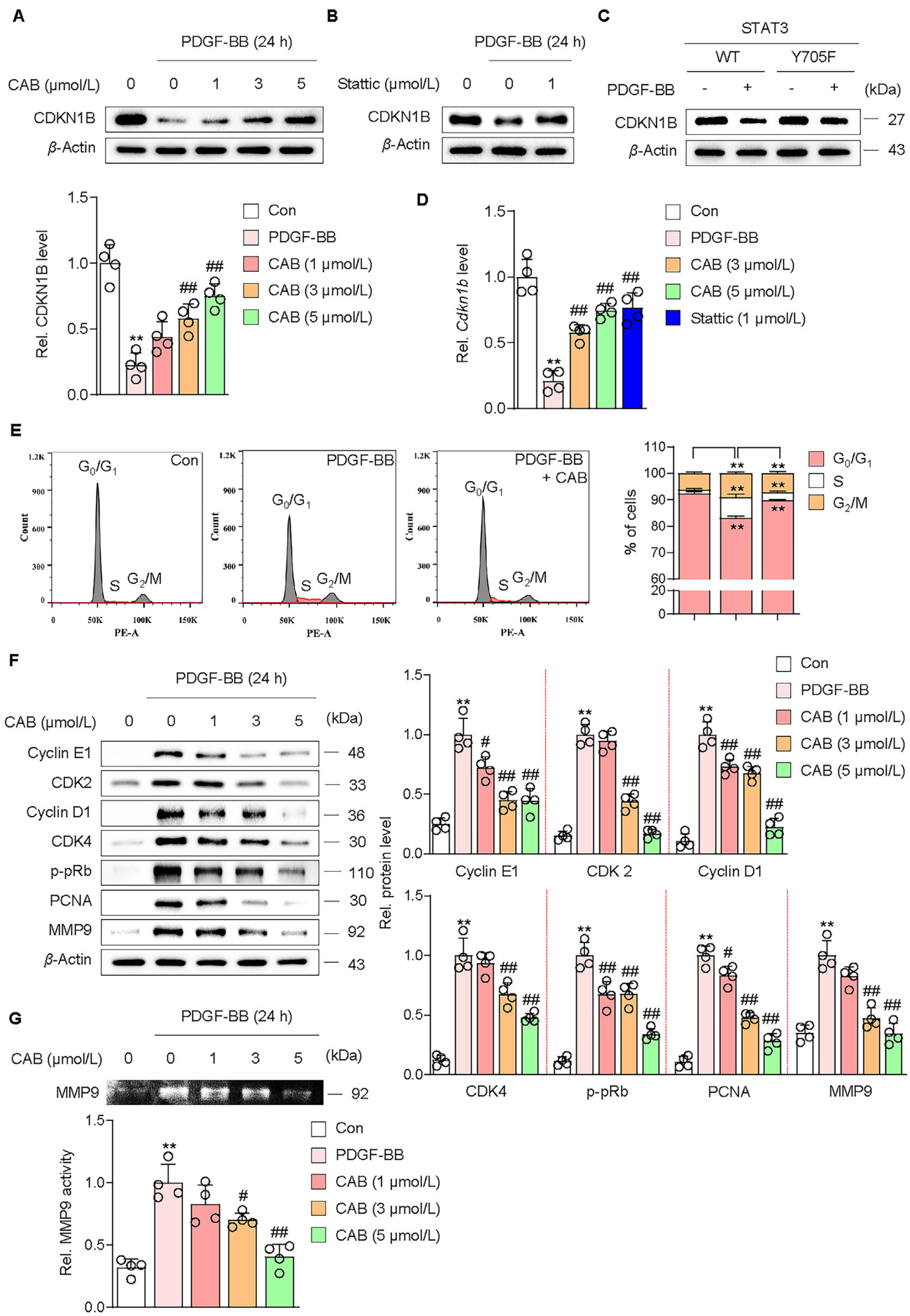

Figure 5 Inhibitory effect of CAB on PDGF-BB induced STAT3/CDKN1B regulation leading to cell cycle arrest and MMP9 repression. Effect of (A) CAB (1−5 μmol/L), (B) stattic (1 μmol/L), (C) STAT3 Tyr705 mutant (Y705F) on CDKN1B expression in the PDGF-BB-induced VSMCs for 24 h (n = 4 per group). WT: wild-type (D) Effect of CAB (1−5 μmol/L) on *Cdkn1b* mRNA expression in the PDGF-BB-induced VSMCs for 24 h (n = 4 per group). (E) Effect of CAB on cell cycle progression in the PDGF-BB-induced VSMCs for 24 h. Representative flow cytometry histograms of cell cycle progression and quantification data (n = 4 per group) are presented. Each shown value was derived by counting at least 10,000 events, and the number of cells in the G_0/G_1, S, and G_2/M phases is expressed as percentages of total cells. (F) Effect of CAB (1−5 μmol/L) on cyclin E1, CDK2, cyclin D1, CDK4, p-Rb, PCNA, and MMP9 expression in the PDGF-BB-induced VSMCs for 24 h (n = 4 per group). (G) Effect of CAB (1−5 μmol/L) on MMP9 activity in the PDGF-BB-induced VSMCs for 24 h. Representative gelatin

3.5. Suppression of STAT3 by CAB leads to CDKN1B-mediated cell cycle arrest and MMP9 suppression

VSMC proliferation and migration are regulated by cell cycle progression and matrix metalloproteinase (MMP) activation[53]. STAT3 regulates the transcription of cell cycle-arresting genes[14,15]. Among cyclin-dependent kinase (CDK) inhibitors, CDKN1B suppresses cell cycle progression and MMP9 activation[54,55].

To verify the effect of CAB on PDGF-BB-induced CDKN1B expression, we examined the level of CDKN1B. As shown in Fig. 5A, CAB dose-dependently restored PDGF-BB-mediated inhibition of CDKN1B expression. In addition, stattic and STAT3 Y705F increased CDKN1B expression in the PDGF-BB-induced VSMCs, indicating that inhibition of STAT3 by CAB increased CDKN1B through transcriptional regulation (Fig. 5B−D, Supporting Information Fig. S6A and S6B).

Next, we investigated whether the CAB-mediated reduction in proliferation was directly linked to cell cycle arrest. PDGF-BB treatment increased cell fraction in the S and G_2/M phases (Fig. 5E). An increase in the G_0/G_1 phase proportion of the CAB-treated VSMCs versus the PDGF-BB-induced VSMCs was observed, indicating that CAB-mediated cell cycle arrest occurred due to disturbed progression from G_0/G_1 to S phase.

As CDKN1B effectors, cyclin and CDK trigger cell cycle progression by sequential intramolecular processes that block retinoblastoma protein (pRb) and activate PCNA in cells entering the G_1 phase[1,56,57]. In addition, MMPs are endopeptidases that regulate vascular structure and remodeling, and MMP9 plays a critical role in VSMC migration and neointima formation[1,4]. As shown in Fig. 5F and G, CAB significantly inhibited PDGF-BB-induced cyclin E1, CDK2, cyclin D1, CDK4, phospho-pRb (p-pRb), PCNA and MMP9 expression, and MMP9 proteolytic activity. Taken together, these results reinforce the understanding that CAB regulates VSMC proliferation and migration *via* the STAT3/CDKN1B pathways.

3.6. CIAPIN1 overexpression counteracts the inhibitory effect of CAB on STAT3-mediated VSMC dedifferentiation, proliferation, and migration

Since CIAPIN1/JAK2/STAT3/KLF4 axis regulated by STAT3 cause alteration of VSMCs proliferation, migration, and dedifferentiation (Fig. 4), we transduced *CIAPIN1* [human CIAPIN1 (hCIA1) at a MOI of 15] into VSMCs. As shown in Fig. 6A and Fig. S6C, hCIAPIN1 and rCIAPIN1 expression was increased by PDGF-BB treatment. Since CIAPIN1 nuclear accumulation was detected in an abnormal proliferative state[58], we examined the CAB-mediated alteration of CIAPIN1 localization. As shown in Fig. 6B, the PDGF-BB-induced increase in CIAPIN1 expression was mainly located in the nucleus. CAB and stattic treatment significantly reduced CIAPIN1 nuclear accumulation, indicating STAT3 regulates CIAPIN1 expression and translocation. Using immunofluorescence, we found that CIAPIN1 significantly accumulated in the nucleus and that transgelin was decreased by PDGF-BB stimulation. In addition, CIAPIN1 overexpression, mainly located in the nucleus, diminished CAB-mediated transgelin restoration, indicating blockade of CAB-induced VSMC differentiation (Fig. 6C). Furthermore, CIAPIN1 overexpression attenuated the inhibitory effect of CAB on PDGF-BB-stimulated VSMC proliferation and migration (Fig. 6D and E). These findings, together with those shown above, reinforce the idea that CIAPIN1 is one of the regulators for STAT3-mediated VSMC dedifferentiation, proliferation, and migration.

3.7. CIAPIN1 overexpression suppresses the inhibitory effect of CAB on neointima formation by affecting identified target alteration

To investigate the physiological effect of CIAPIN1 and CAB on neointima formation after vascular injury, we performed balloon injury and CIAPIN1 overexpression in rat common carotid arteries and administered CAB for 14 days.

Using *in silico* toxicology analysis for favorable drug-like properties, we found that the CAB had no predicted toxicities (Supporting Information Table S2). In addition, CAB administration did not show any side effects, such as diarrhea and weight loss (Supporting Information Fig. S7A). As shown in Fig. S7B, there were no significant changes in the histological morphology of major organs, such as the liver, heart, lung, and kidney. Moreover, there were no alterations in glutamic pyruvic transaminase (GPT/ALT, soluble) or glutamic-oxaloacetic transaminase 1, (GOT1/AST, soluble) levels following CAB administration (Fig. S7C). Since VSMC apoptosis is closely associated with neointima formation, determining plaque stability[59], we also examined the influence of CAB on VSMC apoptosis using TUNEL staining. There were no signs of cell death induction by CAB administration compared with that of the control group, supporting drug safety (Fig. S7D).

CAB administration significantly attenuated balloon injury-induced neointima formation compared to the BI group (Fig. 7A and B). The arterial intimal areas and intima/media ratios were lower in the BI + CAB group than in the BI group, while no differences were noted in the media area and circumference of the external elastic lamina (EEL). Furthermore, we investigated the effect of CAB in mouse carotid ligation model, which induced neointima formation by disturbing flow or increasing shear stress, thus stimulating growth factor secretion and VSMC activation, to determine the therapeutic effect of CAB in vascular dysfunction[60]. The group administrated with CAB in ligated arteries of mouse (LI + CAB) significantly reduced neointima formation by lowering intimal areas and intima/media ratios from ligation-induced carotid artery in comparison with control group (LI + Con) (Fig. S7E and S7F). In addition, CAB administration significantly decreased the expression of PCNA, a proliferative marker, compared with that in the BI group, indicating inhibition of VSMC hyperplasia (Fig. 7C).

Given that CAB regulates CIAPIN1, we performed CIAPIN1 overexpression in arteries and examined the effect of CAB on neointima formation. As shown in Fig. 7A and B, CIAPIN1 overexpression enhanced neointima formation and attenuated the inhibitory effect of CAB on neointima formation, validated by intima area and PCNA staining (Fig. 7C).

Since vascular remodeling causes dysfunction in several cell types, we investigated the localization and expression of CIAPIN1 in arteries. The immunofluorescence results of arteries showed

zymography and quantification data ($n = 4$ per group) for MMP9 activity are presented. P-values were determined by the ANOVA followed by a *post hoc* Bonferroni's test. $^{**}P < 0.01$ *vs*. Con, $^{\#}P < 0.05$ and $^{\#\#}P < 0.01$ *vs*. PDGF-BB. The data are the mean ± SD.

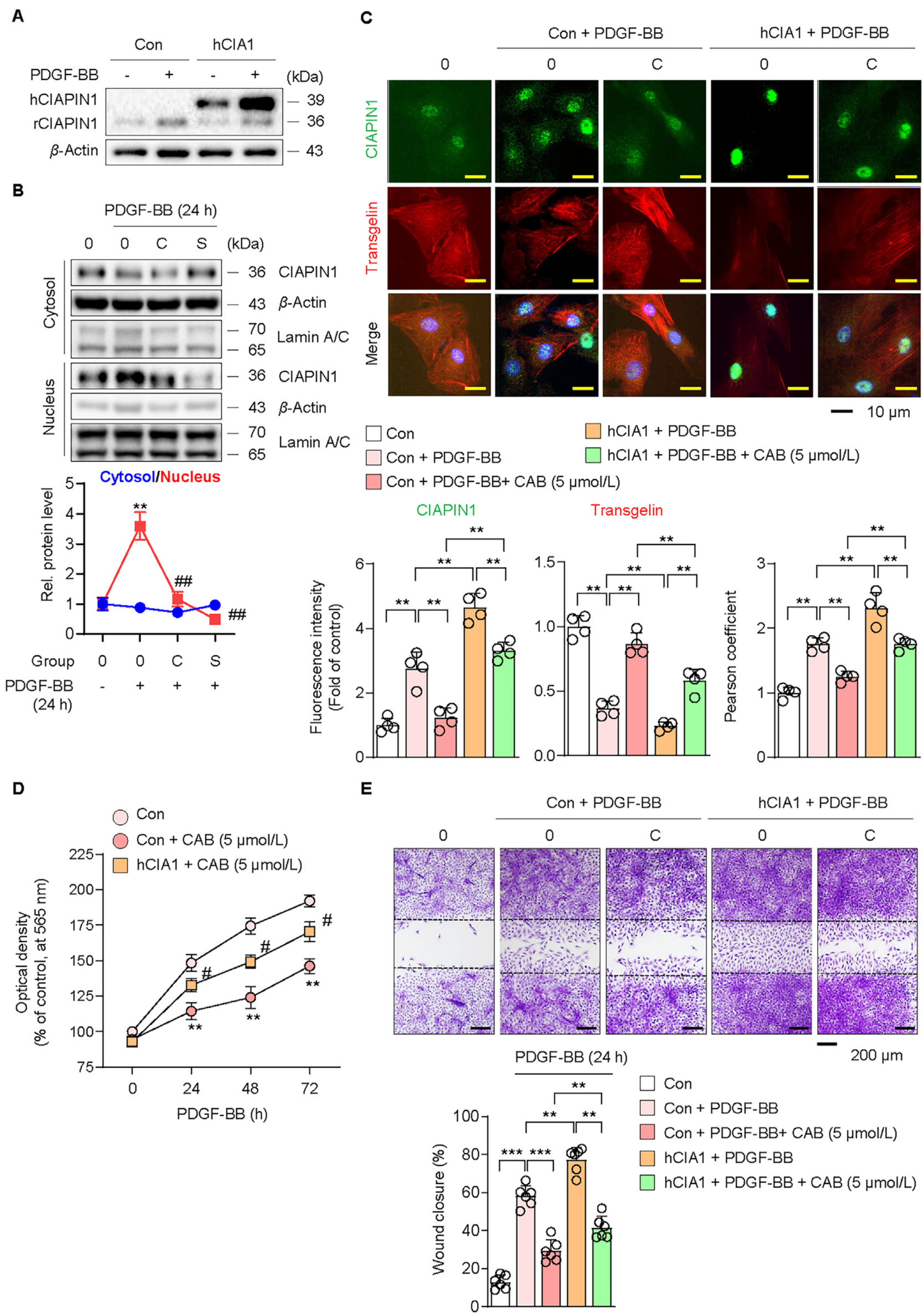

Figure 6 Effect of CIAPIN1 overexpression on CAB-mediated inhibition of VSMC dedifferentiation, proliferation, and migration. (A) Verification of human CIAPIN1 (hCIAPIN1 or hCIA1) transduction in VSMCs using Western blot assay. (B) Effect of CAB and stattic on CIAPIN1 nuclear translocation in the PDGF-BB-induced VSMCs for 24 h. The cells were fractionated into cytosolic and nuclear compartments as described in the Methods section ($n = 4$ per group). P-values were determined by the ANOVA followed by a *post hoc* Bonferroni's test. $^{**}P < 0.01$ *vs*. Con, and $^{\#\#}P < 0.01$ *vs*. PDGF-BB. (C) Fluorescence images (top) and quantification data (bottom) of CIAPIN1 and transgelin in the PDGF-BB-induced VSMCs for 24 h. The fluorescence intensities of FITC (*i.e.*, CIAPIN1) and TRITC (*i.e.*, transgelin) were quantified using ImageJ software. Colocalization of FITC and DAPI (*i.e.*, nuclei) was analyzed using the Pearson correlation coefficient ($n = 4$ per group). Scale bars: 10 μm. P-values were determined by the ANOVA followed by a *post hoc* Bonferroni's test. $^{**}P < 0.01$ *vs*. each group. (D) MTT assay showing the effect of CAB (5 μmol/L) on PDGF-BB-induced CIAPIN1-overexpressing VSMC proliferation at 24, 48 and 72 h ($n = 5$ per group).

abundant CIAPIN1 expression with smooth muscle (SM) α-actin in the neointima region. CAB administration remarkably decreased CIAPIN1 expression, but CIAPIN1 overexpression induced CIAPIN1 expression in the neointima region, indicating CIAPIN1 functions to intima hyperplasia mostly in VSMCs (Fig. 7D).

In VSMCs, CIAPIN1 overexpression attenuated CAB-mediated suppression of JAK2 expression and JAK2 and STAT3 phosphorylation (Fig. 7E and Supporting Information Fig. S8). In addition, CIAPIN1 overexpression attenuated the inhibition of KLF4 and SPP1 expression and the increase in CDKN1B expression by CAB treatment, indicating that CAB inhibits VSMC dedifferentiation, proliferation, and migration *via* CIAPIN1-associated downstream pathways.

Taken together, our results support the conclusion that CAB inhibits STAT3 activation and subsequently attenuates the CIAPIN1/JAK2/STAT3 pathways to affect KLF4-mediated VSMC phenotypic switching and CDKN1B-mediated proliferation and migration.

4. Discussion

VSMC phenotypic switching leads to abnormal cell proliferation and migration and contributes to the development of neointima formation, followed by atherosclerotic progression and vascular remodeling[5]. In the present study, we demonstrated the therapeutic relevance of novel 9*H*-carbazol-3-yl 4-aminobenzoate (CAB) based on the following: (1) CAB suppressed PDGF-BB-induced VSMC dedifferentiation, proliferation and migration; (2) CAB inhibited PDGF-BB-induced STAT3 activation and impeded CIAPIN1/JAK2/STAT3 autoregulatory circuits, affecting their transcription; (3) STAT3 inhibition *via* CAB is critical for KLF4-mediated phenotypic switching and CDKN1B-mediated cell cycle arrest and MMP9 suppression; and (4) STAT3 inhibition by CAB blocked VSMC neointima formation through suppressing the CIAPIN1/JAK2/STAT3 pathways, which was consistent with the *in vitro* results. These findings demonstrate the role of STAT3 on CIAPIN1 regulation in vascular remodeling.

Carbazole is a tricycle compound with two benzene rings fused on either side of a pyrrole core[61]. Although studies initially focused on the fluorescent properties, naturally occurring bioactive carbazole alkaloids were isolated mainly from taxonomically similar plants of the genera *Murraya*, *Flycosmis*, and *Clausena* in the family Rutaceae[62,63]. Since then, carbazole has been considered an important privileged scaffold in drug discovery. Many derivatives with a carbazolic core have been developed, and some of them have shown biological activities due to electrophilic aromatic substitution, oxidative reactions, and alkylation reactions upon binding to the target proteins[64]. Their pharmaceutical potential provides an opportunity to discover and develop drug candidates with antioxidant[65], antiviral[66], antimicrobial[67], and anti-inflammatory properties[68]. We previously reported that murrayafoline A, a carbazole alkaloid isolated from *Glycosmis stenocarpa Guillamin*, inhibited PDGF-BB-induced VSMC cell cycle progression[38]. LCY-2-CHO ([9-(2-chlorobenzyl)-9*H*-Carbazole-3-carbaldehyde]) inhibited inflammatory gene expression inducing heme oxygenase-1 gene expression in VSMCs[68]. Moreover, 3-*N*- or 3-*O*-cinnamoyl carbazole derivatives protected against high-mobility group box 1-mediated vascular disruptive responses in human umbilical vein endothelial cells[23]. In this study, CAB selectively inhibited STAT3 activation by PDGF-BB and suppressed VSMC-mediated neointimal hyperplasia (Figs. 2 and 7, Figs. S2, S5, and S7). Furthermore, we validated the drug-likeness of CAB using PK and toxicity analysis. From the perspective that intracellular PK is converted to pharmacodynamics, the effect of CAB in VSMCs appeared immediately and was maintained for a long time; thus, the PK results provided further evidence of a CAB-mediated therapeutic effect (Fig. 1F). Moreover, toxicity prediction results and *in vitro* and *in vivo* toxicity analysis supported CAB as a safe drug candidate and scaffold (Table S2, Fig. 1C and D, Fig. S7).

Cytokines or growth factors, such as PDGF, bind to their corresponding cell surface receptors[69]. The formation of a dimer complex by these bound receptors initiates the recruitment of JAKs, thereby activating the JAK/STAT signaling pathway through a phosphorylation cascade. The cytoplasmic phosphorylated tyrosine residues of these receptors create a dock for the STAT3 SH2 domain[70]. STAT3 is activated through phosphorylation of Tyr705 located in the SH2 domain. Once activated, phospho-STAT3 monomers interact *via* their SH2 domain to form a homodimer of phospho-STAT3, which then dissociates from cytoplasmic partners and translocates to the nucleus, where it binds to DNA elements within target genes to regulate transcription[71]. Blockade of the SH2 domain of STAT3 using a small-molecule inhibitor can be a potentially promising therapeutic approach in the development of molecularly STAT3 targeted therapies for the treatment of abnormal proliferative disease. Our study showed that CAB interacted with the STAT3 SH2 domains using docking experiments, His-tag pull-down assay, and SPR assay. In addition, CAB inhibited PDGF-BB-induced STAT3 Tyr705 phosphorylation, dimerization, nuclear translocation, and transcriptional activity (Figs. 2 and 3). We investigated the inhibitory effects of CAB in PDGF signaling and STAT3 activation of VSMCs, employing multiple treatment time points with PDGF-BB. Initially, phosphorylation of PDGFR-β, AKT, ERK1/2, p38, and STAT3 has observed around the 15-min time point[72]. Dimerization of the receptor or cytosolic proteins occurred approximately 1 h after phosphorylation[73,74]. Dimerized STAT3 then functioned as a transcription factor in the DNA binding region around 6 h[75]. Subsequently, through STAT3 activation and the downstream gene expression, events such as cell cycle progression, migration, and phenotype switching took place, with related target proteins detected around the 24-h mark[76].

VSMCs can be classified into two major phenotypes: fully differentiated contractile cells responsible for vasocontraction and dedifferentiated synthetic cells consisting of proliferative and migratory cells activated during growth and injury[77]. Notably, switching of the two phenotypes from contractile to synthetic is pivotal for stable plaque formation. Thus, reducing the excessive proliferation and migration of VSMCs *via* phenotypic switching is a therapeutic strategy for atherosclerosis. Our previous study reported that CIAPIN1 accelerates VSMC dedifferentiation through

P-values were determined by the unpaired Student's *t*-test. $^{**}P < 0.01$ *vs*. LV-Con, $^{\#}P < 0.05$ *vs*. LV-Con + CAB (5 μmol/L) for each time. (E) Wound healing assay showing the effect of CAB (5 μmol/L) on PDGF-BB-induced CIAPIN1-overexpressing VSMC migration after 24 h ($n = 5$ per group). *P*-values were determined by the ANOVA followed by a *post hoc* Bonferroni's test. $^{**}P < 0.01$ and $^{***}P < 0.001$ *vs*. each group. The data are the mean ± SD.

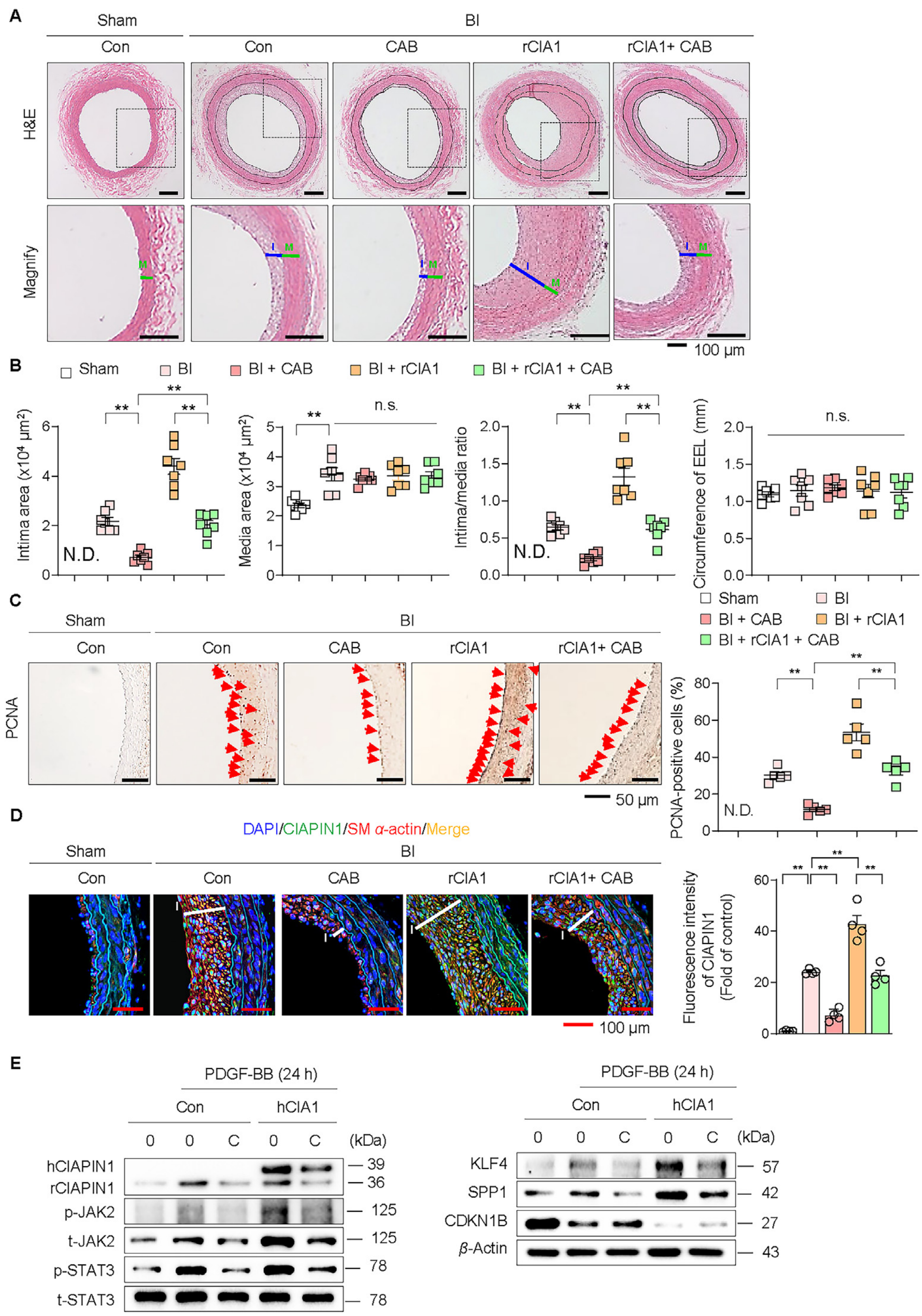

Figure 7 Effect of CAB and CIAPIN1 overexpression on neointima formation. (A) Representative images showing H&E staining in CAB-administered rat carotid arteries 14 days after injury. Sham: sham-operated, BI: balloon-injured, rCIA1: rat CIAPIN1 overexpression, I: intima, M: media. Scale bar: 100 μm. (B) Quantification of the intima and media area, intima/media ratio, and circumference of the external elastic lamina (EEL) in histological sections ($n = 7$ per group). N.D.: not detected. (C) Representative images showing the immunohistochemistry staining for PCNA-positive cells (dark brown, red arrow) and quantification of percentages of stained cells in the sham, BI, and BI with CAB-administered rat carotid arteries 14 days post-injury. Scale bars: 50 μm ($n = 5$ per group). (D) Representative images and quantification of immunofluorescence analysis in rat carotid arteries 14 days post-injury and after CIAPIN1 overexpression and CAB administration. Nuclei were stained with DAPI (blue), CIAPIN1 (FITC, green), and SM α-actin (TRITC, red). Scale bars: 100 μm ($n = 5$ per group). (E) Effect of CAB (5 μmol/L) on CIAPIN1, JAK2, STAT3, KLF4, SPP1 and CDKN1B activation in the PDGF-BB-induced CIAPIN1-overexpressing VSMCs for 24 h. *P*-values were determined by the ANOVA followed by a *post hoc* Bonferroni's test. $^{**}P < 0.01$ *vs*. each group. n.s.: not significant. The data are the mean ± SD.

contractile and synthetic gene regulation under injury conditions[16]. STAT3 inhibition using CAB, stattic and the Tyr705 mutant suppressed CIAPIN1 expression, indicating STAT3 as an upstream molecule and showing that STAT3 regulated CIAPIN1 transcription (Figs. 3 and 4). Interestingly, CIAPIN1 has been reported to be a JAK2 regulator[78], and the CIAPIN1/JAK2/STAT3 pathway can be an autoregulatory circuit from STAT3 activation. In addition, we found that KLF4 is a downstream molecule of CIAPIN1/JAK2/STAT3. Since KLF4 acts as a repressor of myocardin activity and subsequent contractile gene transcription[50], CIAPIN1-mediated KLF4 activation is important evidence of VSMC proliferation and migration (Fig. 7E). While our qPCR and transcriptional data suggest that CAB, as a novel compound, potentially suppresses the CIAPIN1 and KLF4 pathways, the overall transcriptional landscape requires further characterization through bulk RNA-seq to fully profile its effects.

5. Conclusions

In conclusion, this study demonstrated that the compound CAB inhibited vascular intima hyperplasia by affecting VSMC phenotypic switching, proliferation, and migration. In addition, CAB suppressed PDGF-induced STAT3 activation by directly binding to the SH2 domain of STAT3. Moreover, STAT3, target molecules of CAB, play essential roles in CIAPIN1/JAK2/STAT3-mediated KLF4 and CDKN1B regulation in VSMCs. These findings provide new insight into the mechanism by which STAT3 regulates vascular remodeling and molecular links to therapeutic targets for the treatment of atherosclerosis, restenosis, and other vascular proliferative diseases.

Acknowledgments

This study was supported by a National Research Foundation (NRF) grant funded by the Korean government (MSIT, Republic of Korea) (RS-2024-00355169 to Joo-Hui Han, 2022R1A2C2013309 to Chang-Seon Myung) and by Woosuk University (to Joo-Hui Han, Republic of Korea).

Author contributions

Joo-Hui Han: Writing — review & editing, Writing — original draft, Supervision, Project administration, Methodology, Investigation, Funding acquisition, Conceptualization. Jong-Beom Heo: Validation, Formal analysis. Hyung-Won Lee: Visualization, Formal analysis. Min-Ho Park: Validation, Formal analysis. Jangmi Choi: Validation, Formal analysis. Eun Joo Yun: Validation, Formal analysis. Seongpyo Lee: Visualization, Formal analysis. Gyu Yong Song: Visualization, Validation, Supervision. Chang-Seon Myung: Writing — review & editing, Supervision, Funding acquisition.

Conflicts of interest

The authors declare that there is no conflict of interest.

Appendix A. Supporting information

Supporting information to this article can be found online at https://doi.org/10.1016/j.apsb.2024.12.035.

References

1. Basatemur GL, Jorgensen HF, Clarke MCH, Bennett MR, Mallat Z. Vascular smooth muscle cells in atherosclerosis. *Nat Rev Cardiol* 2019;**16**:727—44.
2. Park HS, Han JH, Jung SH, Lee DH, Heo KS, Myung CS. Anti-apoptotic effects of autophagy *via* ROS regulation in microtubule-targeted and PDGF-stimulated vascular smooth muscle cells. *Korean J Physiol Pharmacol* 2018;**22**:349—60.
3. Petsophonsakul P, Furmanik M, Forsythe R, Dweck M, Schurink GW, Natour E, et al. Role of vascular smooth muscle cell phenotypic switching and calcification in aortic aneurysm formation. *Arterioscler Thromb Vasc Biol* 2019;**39**:1351—68.
4. Lacolley P, Regnault V, Nicoletti A, Li Z, Michel JB. The vascular smooth muscle cell in arterial pathology: a cell that can take on multiple roles. *Cardiovasc Res* 2012;**95**:194—204.
5. Bennett MR, Sinha S, Owens GK. Vascular smooth muscle cells in atherosclerosis. *Circ Res* 2016;**118**:692—702.
6. Kim Y, Lee JJ, Lee SG, Jung SH, Han JH, Yang SY, et al. 5,8-Dimethoxy-2-nonylamino-naphthalene-1,4-dione inhibits vascular smooth muscle cell proliferation by blocking autophosphorylation of PDGF-receptor β. *Korean J Physiol Pharmacol* 2013;**17**:203—8.
7. Han JH, Park HS, Lee DH, Jo JH, Heo KS, Myung CS. Regulation of autophagy by controlling Erk 1/2 and mTOR for platelet-derived growth factor-BB-mediated vascular smooth muscle cell phenotype shift. *Life Sci* 2021;**267**:118978.
8. Owens GK, Kumar MS, Wamhoff BR. Molecular regulation of vascular smooth muscle cell differentiation in development and disease. *Physiol Rev* 2004;**84**:767—801.
9. Rivard A, Andres V. Vascular smooth muscle cell proliferation in the pathogenesis of atherosclerotic cardiovascular diseases. *Histol Histopathol* 2000;**15**:557—71.
10. Chen Q, Lv J, Yang W, Xu B, Wang Z, Yu Z, et al. Targeted inhibition of STAT3 as a potential treatment strategy for atherosclerosis. *Theranostics* 2019;**9**:6424—42.
11. Behera R, Kumar V, Lohite K, Karnik S, Kundu GC. Activation of JAK2/STAT3 signaling by osteopontin promotes tumor growth in human breast cancer cells. *Carcinogenesis* 2010;**31**:192—200.
12. Qin S, Zou Y, Zhang CL. Cross-talk between KLF4 and STAT3 regulates axon regeneration. *Nat Commun* 2013;**4**:2633.
13. Hall J, Guo G, Wray J, Eyres I, Nichols J, Grotewold L, et al. Oct 4 and LIF/Stat 3 additively induce Kruppel factors to sustain embryonic stem cell self-renewal. *Cell Stem Cell* 2009;**5**:597—609.
14. Ding BB, Yu JJ, Yu RY, Mendez LM, Shaknovich R, Zhang Y, et al. Constitutively activated STAT3 promotes cell proliferation and survival in the activated B-cell subtype of diffuse large B-cell lymphomas. *Blood* 2008;**111**:1515—23.
15. Liao L, Chen J, Zhang C, Guo Y, Liu W, Liu W, et al. LncRNA NEAT1 promotes high glucose-induced mesangial cell hypertrophy by targeting miR-222-3p/CDKN1B axis. *Front Mol Biosci* 2020;**7**:627827.
16. Han JH, Heo KS, Myung CS. Cytokine-induced apoptosis inhibitor 1 (CIAPIN1) accelerates vascular remodelling *via* p53 and JAK2—STAT3 regulation in vascular smooth muscle cells. *Br J Pharmacol* 2021;**178**:4533—51.
17. Gluszynska A. Biological potential of carbazole derivatives. *Eur J Med Chem* 2015;**94**:405—26.
18. Welsch ME, Snyder SA, Stockwell BR. Privileged scaffolds for library design and drug discovery. *Curr Opin Chem Biol* 2010;**14**:347—61.
19. Caruso A, Iacopetta D, Puoci F, Cappello AR, Saturnino C, Sinicropi MS. Carbazole derivatives: a promising scenario for breast cancer treatment. *Mini Rev Med Chem* 2016;**16**:630—43.
20. Hsu MJ, Chao Y, Chang YH, Ho FM, Huang LJ, Huang YL, et al. Cell apoptosis induced by a synthetic carbazole compound LCY-2-CHO is mediated through activation of caspase and mitochondrial pathways. *Biochem Pharmacol* 2005;**70**:102—12.
21. Saravanabhavan M, Sathya K, Puranik VG, Sekar M. Synthesis, spectroscopic characterization and structural investigations of new

adduct compound of carbazole with picric acid: DNA binding and antimicrobial studies. *Spectrochim Acta A Mol Biomol Spectrosc* 2014; **118**:399−406.

22. Hieda Y, Anraku M, Choshi T, Tomida H, Fujioka H, Hatae N, et al. Antioxidant effects of the highly-substituted carbazole alkaloids and their related carbazoles. *Bioorg Med Chem Lett* 2014;**24**:3530−3.
23. Ku SK, Lee JH, O Y, Lee W, Song GY, Bae JS. Vascular barrier protective effects of 3-*N*- or 3-*O*-cinnamoyl carbazole derivatives. *Bioorg Med Chem Lett* 2015;**25**:4304−7.
24. Haferlach C, Bacher U, Kohlmann A, Schindela S, Alpermann T, Kern W, et al. CDKN1B, encoding the cyclin-dependent kinase inhibitor 1B (p27), is located in the minimally deleted region of 12p abnormalities in myeloid malignancies and its low expression is a favorable prognostic marker in acute myeloid leukemia. *Haematologica* 2011;**96**:829−36.
25. Nair AB, Jacob S. A simple practice guide for dose conversion between animals and human. *J Basic Clin Pharm* 2016;**7**:27−31.
26. Gouma E, Simos Y, Verginadis I, Lykoudis E, Evangelou A, Karkabounas S. A simple procedure for estimation of total body surface area and determination of a new value of Meeh's constant in rats. *Lab Anim* 2012;**46**:40−5.
27. Cheung MC, Spalding PB, Gutierrez JC, Balkan W, Namias N, Koniaris LG, et al. Body surface area prediction in normal, hypermuscular, and obese mice. *J Surg Res* 2009;**153**:326−31.
28. Xie N, Chen M, Dai R, Zhang Y, Zhao H, Song Z, et al. SRSF1 promotes vascular smooth muscle cell proliferation through a Delta133p53/EGR1/KLF5 pathway. *Nat Commun* 2017;**8**:16016.
29. Li G, Xie N, Yao Y, Zhang Y, Guo J, Feng Y, et al. Identification of PI3K regulatory subunit p55gamma as a novel inhibitor of vascular smooth muscle cell proliferation and neointimal formation. *Cardiovasc Res* 2015;**105**:75−85.
30. Holt AW, Tulis DA. Experimental rat and mouse carotid artery surgery: injury & remodeling studies. *ISRN Minim Invasive Surg* 2013; **2013**:167407.
31. Wu JH, Li Y, Zhou YF, Haslam J, Elvis ON, Mao L, et al. Semaphorin-3E attenuates neointimal formation *via* suppressing VSMCs migration and proliferation. *Cardiovasc Res* 2017;**113**:1763−75.
32. Li PF, Dietz R, von Harsdorf R. Reactive oxygen species induce apoptosis of vascular smooth muscle cell. *FEBS Lett* 1997;**404**: 249−52.
33. Gerthoffer WT. Mechanisms of vascular smooth muscle cell migration. *Circ Res* 2007;**100**:607−21.
34. Milo R, Jorgensen P, Moran U, Weber G, Springer M. BioNumbers—the database of key numbers in molecular and cell biology. *Nucleic Acids Res* 2010;**38**:D750−3.
35. Andrae J, Gallini R, Betsholtz C. Role of platelet-derived growth factors in physiology and medicine. *Genes Dev* 2008;**22**:1276−312.
36. He C, Medley SC, Hu T, Hinsdale ME, Lupu F, Virmani R, et al. PDGFRβ signalling regulates local inflammation and synergizes with hypercholesterolaemia to promote atherosclerosis. *Nat Commun* 2015; **6**:7770.
37. Han JH, Lee SG, Jung SH, Lee JJ, Park HS, Kim YH, et al. Sesamin inhibits PDGF-mediated proliferation of vascular smooth muscle cells by upregulating p21 and p27. *J Agric Food Chem* 2015;**63**:7317−25.
38. Han JH, Kim Y, Jung SH, Lee JJ, Park HS, Song GY, et al. Murrayafoline A induces a G0/G1-phase arrest in platelet-derived growth factor-stimulated vascular smooth muscle cells. *Korean J Physiol Pharmacol* 2015;**19**:421−6.
39. Lim CP, Cao X. Regulation of Stat3 activation by MEK kinase 1. *J Biol Chem* 2001;**276**:21004−11.
40. Tkach M, Rosemblit C, Rivas MA, Proietti CJ, Diaz Flaque MC, Mercogliano MF, et al. p42/p44 MAPK-mediated Stat3Ser727 phosphorylation is required for progestin-induced full activation of Stat3 and breast cancer growth. *Endocr Relat Cancer* 2013;**20**:197−212.
41. Wang D, Ali F, Liu H, Cheng Y, Wu M, Saleem MZ, et al. Quercetin inhibits angiotensin II-induced vascular smooth muscle cell proliferation and activation of JAK2/STAT3 pathway: a target based networking pharmacology approach. *Front Pharmacol* 2022;**13**: 1002363.
42. Kurozumi A, Nakano K, Yamagata K, Okada Y, Nakayamada S, Tanaka Y. IL-6 and sIL-6R induces STAT3-dependent differentiation of human VSMCs into osteoblast-like cells through JMJD2B-mediated histone demethylation of RUNX2. *Bone* 2019; **124**:53−61.
43. Rane SG, Reddy EP. JAKs, STATs and Src kinases in hematopoiesis. *Oncogene* 2002;**21**:3334−58.
44. Schreiner SJ, Schiavone AP, Smithgall TE. Activation of STAT3 by the Src family kinase Hck requires a functional SH3 domain. *J Biol Chem* 2002;**277**:45680−7.
45. Zhang T, Kee WH, Seow KT, Fung W, Cao XM. The coiled-coil domain of Stat3 is essential for its SH2 domain-mediated receptor binding and subsequent activation induced by epidermal growth factor and interleukin-6. *Mol Cell Biol* 2000;**20**:7132−9.
46. Chen H, Bian A, Yang LF, Yin X, Wang J, Ti C, et al. Targeting STAT3 by a small molecule suppresses pancreatic cancer progression. *Oncogene* 2021;**40**:1440−57.
47. Ihle JN. STATs: signal transducers and activators of transcription. *Cell* 1996;**84**:331−4.
48. Shankman LS, Gomez D, Cherepanova OA, Salmon M, Alencar GF, Haskins RM, et al. KLF4-dependent phenotypic modulation of smooth muscle cells has a key role in atherosclerotic plaque pathogenesis. *Nat Med* 2015;**21**:628−37.
49. Liao XH, Wang N, Zhao DW, Zheng DL, Zheng L, Xing WJ, et al. STAT3 protein regulates vascular smooth muscle cell phenotypic switch by interaction with myocardin. *J Biol Chem* 2015;**290**: 19641−52.
50. Pipes GC, Creemers EE, Olson EN. The myocardin family of transcriptional coactivators: versatile regulators of cell growth, migration, and myogenesis. *Genes Dev* 2006;**20**:1545−56.
51. Wirka RC, Wagh D, Paik DT, Pjanic M, Nguyen T, Miller CL, et al. Atheroprotective roles of smooth muscle cell phenotypic modulation and the TCF21 disease gene as revealed by single-cell analysis. *Nat Med* 2019;**25**:1280−9.
52. Mack CP. Signaling mechanisms that regulate smooth muscle cell differentiation. *Arterioscler Thromb Vasc Biol* 2011;**31**:1495−505.
53. Grootaert MOJ, Bennett MR. Vascular smooth muscle cells in atherosclerosis: time for a re-assessment. *Cardiovasc Res* 2021;**117**: 2326−39.
54. Razavipour SF, Harikumar KB, Slingerland JM. p27 as a transcriptional regulator: new roles in development and cancer. *Cancer Res* 2020;**80**:3451−8.
55. Mizuma M, Katayose Y, Yamamoto K, Shiraso S, Sasaki T, Yabuuchi S, et al. Up-regulated p27Kip1 reduces matrix metalloproteinase-9 and inhibits invasion of human breast cancer cells. *Anticancer Res* 2008;**28**:2669−77.
56. Lee JJ, Lee JH, Cho WK, Han JH, Ma JY. Herbal composition of *Cinnamomum cassia, Pinus densiflora, Curcuma longa* and *Glycyrrhiza glabra* prevents atherosclerosis by upregulating p27 (Kip1) expression. *BMC Complement Altern Med* 2016;**16**:253.
57. Lee JJ, Lee JH, Yim NH, Han JH, Ma JY. Application of galangin, an active component of *Alpinia officinarum* Hance (Zingiberaceae), for use in drug-eluting stents. *Sci Rep* 2017;**7**:8207.
58. Cai X, Wang J, Xin X. CIAPIN1 nuclear accumulation predicts poor clinical outcome in epithelial ovarian cancer. *World J Surg Oncol* 2012;**10**:112.
59. Yu H, Clarke MC, Figg N, Littlewood TD, Bennett MR. Smooth muscle cell apoptosis promotes vessel remodeling and repair *via* activation of cell migration, proliferation, and collagen synthesis. *Arterioscler Thromb Vasc Biol* 2011;**31**:2402−9.
60. Korshunov VA, Berk BC. Flow-induced vascular remodeling in the mouse: a model for carotid intima-media thickening. *Arterioscler Thromb Vasc Biol* 2003;**23**:2185−91.

61. Schmidt AW, Reddy KR, Knolker HJ. Occurrence, biogenesis, and synthesis of biologically active carbazole alkaloids. *Chem Rev* 2012;**112**:3193−328.
62. Thomas KR, Lin JT, Tao YT, Ko CW. Light-emitting carbazole derivatives: potential electroluminescent materials. *J Am Chem Soc* 2001;**123**:9404−11.
63. Knolker HJ, Reddy KR. Isolation and synthesis of biologically active carbazole alkaloids. *Chem Rev* 2002;**102**:4303−427.
64. Kobayashi M, Kuzuyama T. Recent advances in the biosynthesis of carbazoles produced by actinomycetes. *Biomolecules* 2020;**10**:1147.
65. Alayrac C, Schollmeyer D, Witulski B. First total synthesis of antiostatin A1, a potent carbazole-based naturally occurring antioxidant. *Chem Commun* 2009;**12**:1464−6.
66. Caruso A, Ceramella J, Iacopetta D, Saturnino C, Mauro MV, Bruno R, et al. Carbazole derivatives as antiviral agents: an overview. *Molecules* 2019;**24**:1912.
67. Unver Y, Suleymanoglu N, Ustabas R, Bektas KI, Bektas E, Guler HI. 3-(5-(1*H*-Imidazole-1-yl) pent-1-en-1-yl)-9-ethyl-9*H*-carbazole: synthesis, characterization (IR, NMR), DFT, antimicrobial-antioxidant activities and docking study. *J Biomol Struct Dyn* 2022;**40**:12990−3000.
68. Ho FM, Kang HC, Lee ST, Chao Y, Chen YC, Huang LJ, et al. The anti-inflammatory actions of LCY-2-CHO, a carbazole analogue, in vascular smooth muscle cells. *Biochem Pharmacol* 2007;**74**:298−308.
69. Aaronson DS, Horvath CM. A road map for those who don't know JAK−STAT. *Science* 2002;**296**:1653−5.
70. Zhang X, Yue P, Fletcher S, Zhao W, Gunning PT, Turkson J. A novel small-molecule disrupts Stat3 SH2 domain-phosphotyrosine interactions and Stat3-dependent tumor processes. *Biochem Pharmacol* 2010;**79**:1398−409.
71. Zhang X, Guo A, Yu J, Possemato A, Chen Y, Zheng W, et al. Identification of STAT3 as a substrate of receptor protein tyrosine phosphatase T. *Proc Natl Acad Sci U S A* 2007;**104**:4060−4.
72. Park HS, Quan KT, Han JH, Jung SH, Lee DH, Jo E, et al. Rubiarbonone C inhibits platelet-derived growth factor-induced proliferation and migration of vascular smooth muscle cells through the focal adhesion kinase, MAPK and STAT3 Tyr(705) signalling pathways. *Br J Pharmacol* 2017;**174**:4140−54.
73. Qi X, Li M, Zhang XM, Dai XF, Cui J, Li DH, et al. Trichothecin inhibits cancer-related features in colorectal cancer development by targeting STAT3. *Molecules* 2020;**25**:2306.
74. Kim Y, Han JH, Yun E, Jung SH, Lee JJ, Song GY, et al. Inhibitory effect of a novel naphthoquinone derivative on proliferation of vascular smooth muscle cells through suppression of platelet-derived growth factor receptor β tyrosine kinase. *Eur J Pharmacol* 2014;**733**:81−9.
75. Im JY, Kim BK, Lee KW, Chun SY, Kang MJ, Won M. DDIAS promotes STAT3 activation by preventing STAT3 recruitment to PTPRM in lung cancer cells. *Oncogenesis* 2020;**9**:1.
76. Park S, Kim JK, Oh CJ, Choi SH, Jeon JH, Lee IK. Scoparone interferes with STAT3-induced proliferation of vascular smooth muscle cells. *Exp Mol Med* 2015;**47**:e145.
77. Kolodgie FD, Burke AP, Farb A, Gold HK, Yuan J, Narula J, et al. The thin-cap fibroatheroma: a type of vulnerable plaque: the major precursor lesion to acute coronary syndromes. *Curr Opin Cardiol* 2001;**16**:285−92.
78. Shibayama H, Takai E, Matsumura I, Kouno M, Morii E, Kitamura Y, et al. Identification of a cytokine-induced antiapoptotic molecule anamorsin essential for definitive hematopoiesis. *J Exp Med* 2004;**199**:581−92.